2013 European Control Conference (ECC)
July 17-19, 2013, Zürich, Switzerland.

Improving High Speed Road-Holding Using Actively Controlled Aerodynamic Surfaces

M. Corno, S. Bottelli, G. Panzani, M. Tanelli, C. Spelta, S.M. Savaresi

Abstract— **Semi-active and active suspension technologies have shown that vehicles road holding can be enhanced, but any such improvement implies decreasing the overall comfort. In this paper, we introduce the use of active aerodynamic surfaces to improve vehicle road-holding without affecting comfort. An $\mathcal{H}_\infty$ closed-loop controller is developed to minimize the tire deflection variations, which are responsible for the vehicle bad road holding. The controller is designed on a quarter-car model. Extensive simulations on a multi-body vehicle simulation suit assess the performance of the proposed control scheme, and an exhaustive sensitivity analysis shows the role of road roughness, velocity and airfoil design.**

I. Introduction

Improving riding quality is one of the most challenging and interesting topics in automotive research. To this end, car manufacturers have focused on the suspension system and developed several active or semi-active actuators and control strategies. In the past few years, the decreasing cost of electromechanical actuators has, however, opened new paths to face the challenge. Active aerodynamic surfaces represent an alternative and effective solution to the issue. In academic research, active aerodynamics surfaces, have been successfully employed to improve comfort [1] and handling [2]. Industrially, they are employed in high-end cars to improve braking as in the Pagani Huayra and in other premium vehicles to improve engine cooling and thus efficiency.

Riding quality can be better articulated in three categories:

- *Comfort*, the vehicle aptitude for filtering road roughness. It is usually linked to the chassis vertical accelerations;
- *Handling*, the vehicle aptitude for controlling the lateral stability, especially during cornering;
- *Road Holding*, the vehicle aptitude for tackling uneven road profiles without wheel detachment. Road holding is strictly related to ride safety as a good road holding deliver higher and more uniform tyre forces (for example during braking).

In this paper costs and benefits of using active aerodynamic surfaces to improve road holding will be analyzed.

Road holding can be increased by minimizing the tire contact force variations (see [3], [4]), which result directly from the tire deflection variations. Traditionally, road holding is managed and controlled through suspension tuning and control (either active or semi-active suspensions). To date the best known example of suspension-related road holding improving active strategy is the so-called ground-hook. In its semi-active implementation, It simulates a fictitious damper between the wheel center and the road. The ground-hook strategy has been shown to marginally improve road holding at the cost of comfort. The suspension, by exerting a force between the chassis and the wheel, inevitably couples the two masses: when an action is performed on one a reaction affects the others. A trade-off thus arises. In this work, it will be shown how active aerodynamic surfaces, by generating a force directly on the wheel axes, can overcome this trade-off, increasing road holding without affecting comfort.

The paper is structured as follows. In Section II a linear quarter car dynamic model is set up in order to study the overall system. The aerodynamic properties of the airfoil are studied, as well as the road input, which is required to be as realistic as possible. A method to evaluate the road holding improvement is also defined. In Section III, a $\mathcal{H}_\infty$ controller is developed, and the expected performance is defined in terms of road holding improvement and non-interaction with comfort. Finally, the simulation results are described in Section IV and sensitivity analyses carried out.

II. Problem Set Up

In this section the quarter car (Section II-A) and the aerodynamic actuator models (Section II-B) are studied. Subsequently, an analysis on the road profile design (Section II-C) and the evaluation methods for the proposed system (Section II-D) is conducted.

A. Dynamic vehicle model

The vertical dynamics of the vehicle can be well described by the quarter car model, which is modified to include the effect of the aerodynamic surface. To do so one input is added to the classic quarter car model. The resulting equations are:

$$\begin{cases} M\ddot{z}(t) = -c(\dot{z}(t) - \dot{z}_t(t)) - k(z(t) - z_t(t)) \\ m\ddot{z}_t(t) = c(\dot{z}(t) - \dot{z}_t(t)) + k(z(t) - z_t(t)) \\ \qquad\qquad -k_t(z_t(t) - z_r(t)) + F_{lift}(t) \\ F_{lift}(t) = \frac{1}{2}\rho V^2 S\, C_{lift}(\alpha, t) = k_v C_{lift}(\alpha, t). \end{cases} \tag{1}$$

In system (1), z, $\dot{z}$ and $\ddot{z}$ refer to the sprung mass vertical position, speed and acceleration, while z_t, $\dot{z}_t$ and $\ddot{z}_t$ are respectively the wheel center vertical position, speed and acceleration. The two inputs are the road height z_r and the aerodynamic lift F_{lift}, which is defined by a constant k_v times

M. Corno, S. Bottelli, G. Panzani, M. Tanelli and S.M. Savaresi are with the Dipartimento di Elettronica e Informazione, Politecnico di Milano, Milan, Italy. <surname>@elet.polimi.it. C. Spelta is with Dipartimento di Ingegneria dell'Informazione e metodi Matematici Universit degli Studi di Bergamo. This project was supported by Honda R&D Europe (Deutschland) GmbH in line with the Honda Initiation Grant Europe (HIGE)

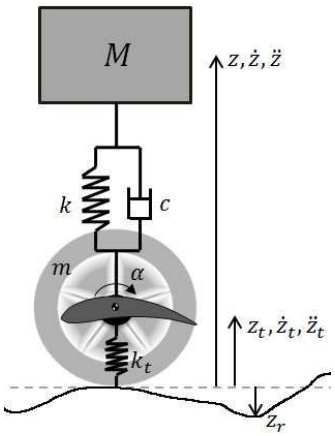

Fig. 1. Quarter car model.

TABLE I

QUARTER CAR PARAMETERS

Symbol	Description	Value	Unit
M	Sprung mass	310	kg
m	Unsprung mass	40	kg
c	Damper stiffness	2500	Ns/m
k	Spring constant	$3{\cdot}10^4$	N/m
k_t	Tire equivalent spring constant	$2{\cdot}10^5$	N/m
ρ	Air density	1.275	kg/m^3
V	Vehicle speed	200	km/h
S	Airfoil surface	0.1	m^2

the control variable C_{lift} (an analysis on the aerodynamic coefficients will be done in Section II-B). See Fig. 1 for further details. The vehicle is supposed to drive at constant speed. Table I shows the main vehicle parameters.

From system (1), 4 fundamental transfer functions are computed:

$$G_1(s) = \frac{z_{def_t}(s)}{C_{lift}(s)} = \frac{4.63(s^2 + 8.06s + 96.77)}{(s^2 + 6.46s + 90.58)(s^2 + 64.1s + 5342)}$$
$$G_2(s) = \frac{\ddot{z}(s)}{C_{lift}(s)} = \frac{37.34s^2(s + 12)}{(s^2 + 6.46s + 90.58)(s^2 + 64.1s + 5342)} \quad (2)$$

$$H_{1OL}(s) = \frac{z_{def_t}(s)}{z_r(s)} = \frac{s^2(s + 55.23)(s + 15.33)}{(s^2 + 6.46s + 90.58)(s^2 + 64.1s + 5342)}$$
$$H_{2OL}(s) = \frac{\ddot{z}(s)}{\ddot{z}_r(s)} = \frac{40322.58(s + 12)}{(s^2 + 6.46s + 90.58)(s^2 + 64.1s + 5342)} \quad (3)$$

The expressions in (3) are the well-known quarter car transfer functions from road vertical acceleration to vertical chassis acceleration and from road height to tire deflection. The transfer functions in (2) represent the effect of the controllable input; their Bode diagrams are shown in Fig. 2. In particular, $G_1(s)$ is the transfer function from lift coefficient to tire deflection, and $G_2(s)$ is the transfer function from lift coefficient to chassis vertical acceleration.

It is possible to observe that in $G_1(s)$ the wheel resonance (at around 10 Hz) is clearly visible, while the body resonance

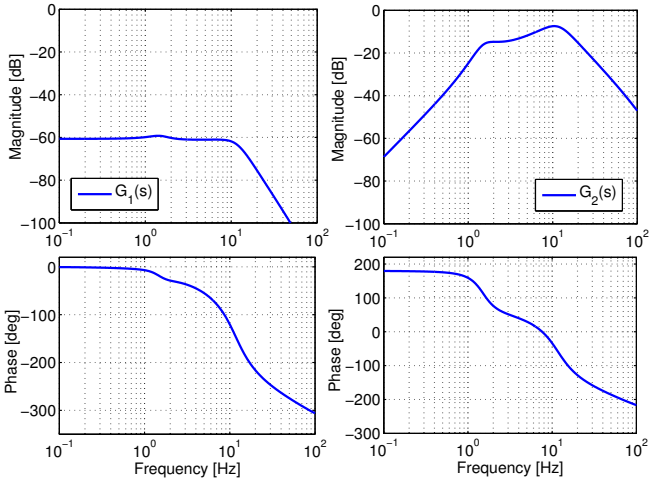

Fig. 2. Transfer functions $G_1(s)$ and $G_2(s)$.

(at around 1 Hz) is barely visible. In $G_2(s)$ both resonances are recognizable.

B. Aerodynamic actuator model

Both upward and downward forces need to be generated in order to control the vertical dynamics, consequently a symmetrical airfoil is preferred. Throughout this dissertation the NACA0014 will be analyzed, whose characteristics are defined according to the NACA protocol [5]. However, the proposed methods can be readily applied to other symmetrical airfoils. The lift and drag forces, as well as the pitching moment, obey the following equations:

$$F_{lift} = \frac{1}{2}\rho V^2 S C_{lift}(\alpha)$$
$$F_{drag} = \frac{1}{2}\rho V^2 S C_{drag}(\alpha) \quad (4)$$
$$M_{pitch} = \frac{1}{2}\rho V^2 S c C_{pitch}(\alpha)$$

where ρ is the air density, V is the air flow speed, S is the airfoil surface, c is the airfoil chord, α is the angle of attack and C_{lift}, C_{drag} and C_{pitch} are coefficients which depend on Reynolds number, angle of attack, airfoil shape and roughness. After having defined the position and the airfoil characteristics, the three coefficients depend only on the angle of attack (see Fig. 3).

As shown in figure, the available lift force is limited. The maximum lift force is generated at $\alpha = 15°$. Higher values of angle of attack won't be used, in order to prevent the airfoil to exceed its stall point. The saturation of the angle of attack introduces a non-linearity in (1). It should be noted that the drag coefficient is negligible compared to the other coefficients.

According to the previous model, the aerodynamic forces statically depend on the angle of attack. This model may fail under dynamic excitation; to account for this a more accurate model is employed. C_{lift}, C_{drag} and C_{pitch} are modeled by the dynamical system in (5), where $C_{*_\alpha}(t)$ is the slope of the statically mapped lift, drag or pitch coefficient in

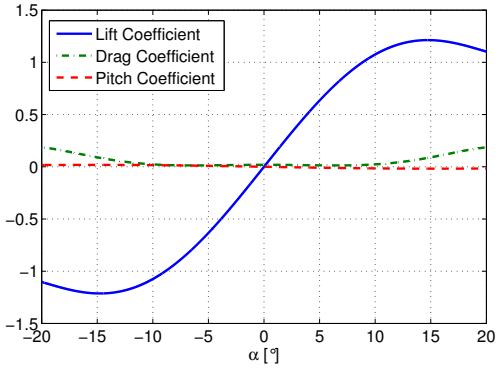

Fig. 3. Lift, drag and pitch coefficients.

correspondence to the input α, and $A_1 = 0.165$, $A_2 = 0.335$, $b_1 = 0.0455$, $b_2 = 0.3$, according to Jones' approximation (see [6] for more details).

$$\begin{cases} \begin{bmatrix} \dot{x}_1(t) \\ \dot{x}_2(t) \end{bmatrix} = \frac{2V(t)}{c} \begin{bmatrix} -b_1 & 0 \\ 0 & -b_2 \end{bmatrix} \begin{bmatrix} x_1(t) \\ x_2(t) \end{bmatrix} + \begin{bmatrix} 1 \\ 1 \end{bmatrix} \alpha(t) \\ C_*(t) = C_{*_\alpha}(t) \frac{2V(t)}{c} \begin{bmatrix} A_1 b_1 & A_2 b_2 \end{bmatrix} \begin{bmatrix} x_1(t) \\ x_2(t) \end{bmatrix} \end{cases} \tag{5}$$

The airfoil number and position is now discussed: neglecting, for now, any technological issue, the airfoils are considered connected to the front and rear axles. Airfoils directly installed on the sprung mass can also be used, but it can be shown that they are less effective in enhancing the vehicle road holding. In order to provide a better attenuation of the tire contact force variations, 4 actuators are employed, one for each corner. The airfoil dimension has been chosen considering its encumbrance and the position in which it has to be installed, but also stressing the fact that the lift force is directly related to the airfoil surface. A good compromise seems to be 0.1 m^2, which leads to a maximum lift force of 130 N (at reference vehicle speed = 200 km/h) for a single airfoil (a more thorough analysis of the airfoil design is carried out in Section IV. This architecture needs to be controlled by using 4 independent actuators, each independently controlled. It will be shown that the controller developed based on the linear quarter car SISO model provides good performance on the full car model.

C. Road Profile

In order to investigate the vehicle response to the excitation coming from the road a realistic road profile has to be determined. The road profile is generated by the following dynamic system (see [7] for details):

$$\begin{gathered} z_r(t) = \frac{1}{s + \alpha_r v} u(t) \\ u(t) \sim WN \\ E[u(t)u(t-\tau)] = 2\alpha_r v \sigma^2 \delta(\tau) \end{gathered} \tag{6}$$

where σ^2 is the variance of the road irregularities, α_r is a coefficient depending on the shape of road irregularities (α_r = 0.15 for standard asphalt), v is the vehicle speed, $\delta(\tau)$ is the Dirac delta function and $E[\cdot]$ is the mean operator. In tuning parameter σ^2, the International Roughness Index (IRI) standard [8] is used. A road IRI is a dimensionless number which measures the road profile roughness: $IRI = 0$ implies a perfectly flat road, while higher IRI values refer to rougher road profiles. The IRI value is computed by equation (7), in which a known quarter car (the Golden Car) is supposed to drive along the road profile at constant speed of 80 km/h. The suspension deflection module is evaluated and integrated over the road length L.

$$IRI = \frac{\int_0^{t_{end}} \left| z_{body}(t) - z_{wheel}(t) \right| dt}{L} \tag{7}$$

The nominal σ^2 has been chosen such that the resulting road has $IRI = 3.5$, which corresponds to a medium-to-older pavement, that is supposed to be driven at 100 km/h. Less maintained pavements will be simulated ($IRI = 5$), as well as smoother ones ($IRI = 2$).

D. Performance Indexes

In this dissertation, road holding is evaluated by considering the tire deflection ($z_{def_t} = z_t - z_r$) minimization problem. Since the system is non linear, the approximate transfer function between the road input and the tire deflection is analyzed, by computing input and output power spectral density $G_{z_r}(f)$ and $G_{z_{def_t}}(f)$. The approximate frequency response is given by:

$$F_{z_{def_t}}(f) = \frac{G_{z_{def_t}}(f)}{G_{z_r}(f)} \tag{8}$$

Let's define, as in [4], the function $\mathscr{C} : \mathbb{R} \times \mathbb{R} \times \mathbb{R} \to \mathbb{R}$ as follows:

$$\mathscr{C}(X, \underline{f}, \overline{f}) = \int_{\underline{f}}^{\overline{f}} |X(f)|^2 \, \mathrm{d}f. \tag{9}$$

Consequently, the road holding criterion J_{RH} is determined by equation (10).

$$J_{RH} = \frac{\mathscr{C}(F_{z_{def_t}}, 0, 20)}{\mathscr{C}(F_{z_{def_t}}^{nom}, 0, 20} \tag{10}$$

Conversely, the comfort-oriented criterion is computed as

$$\begin{gathered} F_c(f) = \frac{G_{\ddot{z}}(f)}{G_{\ddot{z}_r}(f)} \\ J_C = \frac{\mathscr{C}(F_c, 0, 20)}{\mathscr{C}(F_c^{nom}, 0, 20)} \end{gathered} \tag{11}$$

where $G_{\ddot{z}}(f)$ and $G_{\ddot{z}_r}(f)$ are the power spectral densities of the chassis vertical acceleration and the road vertical acceleration. It is possible to analyze the comfort road holding trade-off through the normalized performance diagram (Fig. 4), in which every point has coordinates (J_C,J_{RH}) and it is related to a different quarter car configuration. In this example the passive suspension curve (each point related to different passive damper coefficient) is noted, as well as two

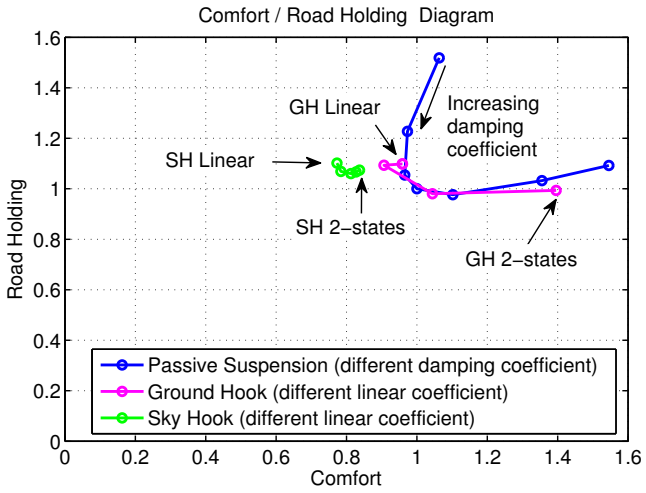

Fig. 4. Comfort - Road Holding Diagram. Curves related to passive suspensions, sky-hook and ground hook are shown.

well known semi-active suspension algorithms, sky hook and ground hook. Observe that it is impossible to increase road holding without affecting comfort [4].

The use of actively controlled aerodynamic surfaces can solve this trade-off; the generated lift force is an external force that acts on the wheel without any direct influence on the chassis (in contrast to what happens with a generic suspension). Seen in the trade-off plane, this application aims at moving downward vertically, starting from the point referred to the nominal passive suspension (1,1).

III. Control System Design

In this section the design of the control system is analyzed. The control system is tuned on the quarter car linear model. A closed-loop controller is designed, and a frequency domain investigation of the road holding and comfort expected performance carried out.

The control scheme of a single corner is shown in Fig. 5. It is noted how the desired value for the tire deflection is 0. The transfer functions $G_1(s)$ and $H_{1OL}(s)$ have already been introduced in Section II-A. The feedback variable is z_t, which is the tire deflection. Different methods based on Kalman filtering exist to estimate it (see [9] and [10]).

The goal of the $\mathcal{H}_\infty$ controller [11] $R(s)$ is to provide a good attenuation over the frequency range where the disturbance is more damaging (around the wheel resonance). Therefore the main requirement is on the sensitivity function $S(s)$:

$$S(s) = \frac{1}{1 + G_1(s)R(s)A(s)} \tag{12}$$

$$\|W_s(s)S(s)\|_\infty \leq 1 \tag{13}$$

$$W_s(s) = \frac{s(s+\omega_{12})^3(s+\omega_{21})^3}{(s+\omega_1)^3(s+\omega_2)^3(s+10^{-4})} \tag{14}$$

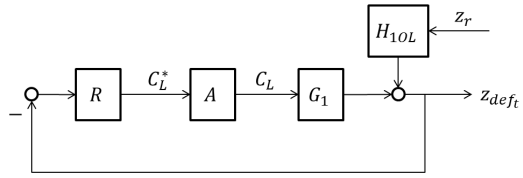

Fig. 5. Closed-loop control scheme.

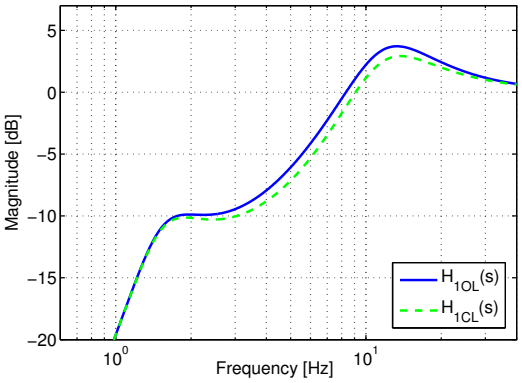

Fig. 6. Disturbance rejection: $\frac{z_{def_t}(s)}{z_r(s)}$ in open and closed-loop.

where $\omega_1 \leq \omega_{12} \leq \omega_{21} \leq \omega_2$. Zeros and poles values should be tuned in order to obtain a good rejection in an appropriate frequency range. The choice of $W_s(s)$ is based on the observation that linearizing model (5) around $\alpha = 0°$, the actuator model can be approximated by low pass at $f_c \sim 10Hz$. This limit has been considered as a performance limit to avoid exciting aerodynamic nonlinearities. It has been thus chosen to roll-off $W_s(s)$ at 10Hz. The chosen parameters are: $\omega_1 = 5 \cdot 2\pi$, $\omega_{12} = 6.2 \cdot 2\pi$, $\omega_{21} = 8.06 \cdot 2\pi$ and $\omega_2 = 10 \cdot 2\pi$. For the same reason, the actuator $A(s)$ has been modeled by using a gray box approach, resulting in 2nd order low pass filter with $f_c = 10Hz$.

The resulting closed-loop road disturbance rejection performance, defined as

$$H_{1CL}(s) = H_{1OL}(s)S(s), \tag{15}$$

is compared to the open-loop one in Fig. 6. If the saturations are neglected, the control system is able to reject the disturbance at the critical wheel hop resonance frequency.

The analysis of the transfer functions from road vertical acceleration to chassis vertical acceleration (with $(H_{2CL}(s))$ and without $(H_{2OL}(s))$ the controller) concludes the linear domain analysis of the proposed controller. A scheme showing the interconnections between the two variables is represented in Fig. 8, from which it can be concluded that

$$H_{2CL}(s) = \frac{\ddot{z}(s)}{\ddot{z}_r(s)} = H_{2OL}(s) - \frac{G_2(s)R(s)A(s)H_{1OL}(s)}{s^2(1 + G_1(s)R(s)A(s))}. \tag{16}$$

Fig. 7 shows that the closed-loop control system has no negative influence on the chassis vertical acceleration, and consequently on comfort.

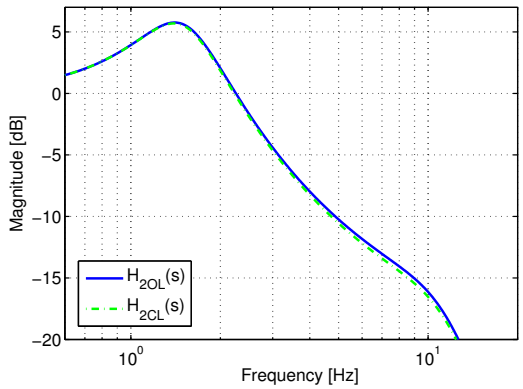

Fig. 7. Interaction analysis: $\frac{\ddot{z}(s)}{\ddot{z}_r(s)}$ in open and closed-loop.

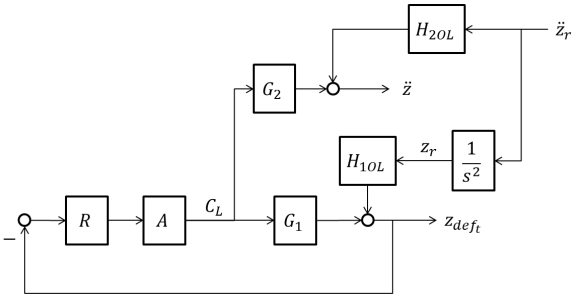

Fig. 8. Extended control scheme.

IV. Simulation Results

The proposed controller has been simulated using Carsim, an accurate multi-body vehicle simulator. Both the quarter car and the full car model have been analyzed. It the following, where not otherwise specified, we will refer to the full car model results.

Each corner has been equipped with an airfoil and a controller, and sensors measure the requested feedback variables. The dynamic model of the airfoil has been used (see Section II-B). In order to verify the efficacy and the robustness of the developed system, three different tests have been set up. The following results are related only to the front left corner, similar results are obtained for the other corners. The indicated power is also associated to one corner. In Table II, III and IV a brief summary is represented, and the information on the requested power is given. In the tables the percentages are positive in the direction of an improvement of the cost function. In the shown trade-off maps, the point corresponding to (1,1) is recomputed for each driving condition, this means that the values should not be used as an indication of the overall absolute performance, but rather as a relative comparison of the improvement introduced by the actively controlled aerodynamic surfaces.

The first test goal is to show what happens if the vehicle travels at different velocities. From Fig. 9, it is noted that the road holding performance is enhanced, testing different velocities from 150km/h to 250km/h. The road is designed in order to have IRI=3.5. As expected, higher velocities improve the effectiveness of the proposed method as the

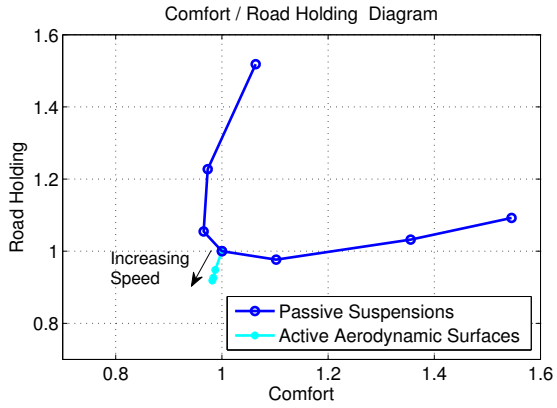

Fig. 9. Comfort - Road Holding diagram for different vehicle velocities.

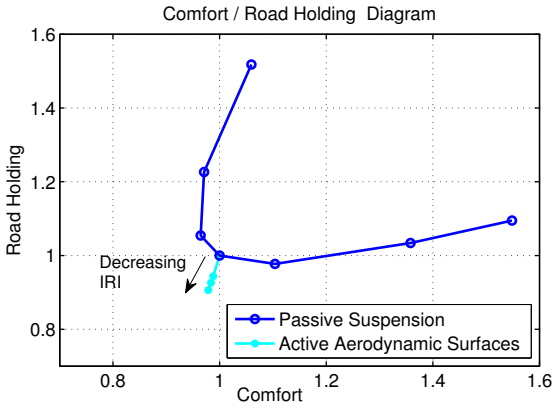

Fig. 10. Comfort - Road Holding diagram for different road roughnesses.

system better exploits the aerodynamic properties of the airfoil. Not that the improvement does not grow linearly with the speed, since the vehicle has to face higher stress from the roadway as the speed increases. This is also the reason why the power requirement is significantly larger at high speed. For all velocities, the comfort performance is slightly improved.

The second test aims at simulating roads with different roughnesses, sweeping IRIs from 2 to 5, at 200km/h. The results are shown in Fig 10. As the road roughness increases, the road-holding performance decreases. In fact high variations of the input variable lead to high variation of the control variable. In so doing, it gets saturated more often reducing performance in a quasi-linear relationship. The requested power is higher, because the actuator employed the full actuation range. Also in this test the comfort performance is slightly improved.

The purpose of the third test is to investigate the impact of the airfoil surface on the road holding results. The analyzed surfaces have been chosen in a reasonable range (from $0.05m^2$ to $0.15m^2$). Increasing the surface it is possible to improve the road holding performance of the system, by means of a small actuation power difference (see Fig. 11 for details). Again, it is shown that the passenger's comfort is slightly increased.

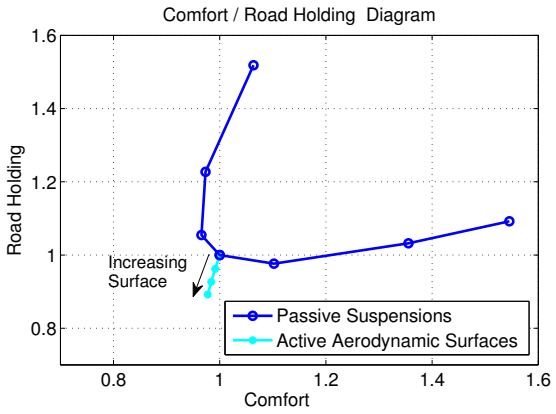

Fig. 11. Comfort - Road Holding diagram for different airfoil surfaces.

TABLE II

FULL CAR RESULTS: DIFFERENT VELOCITIES (FRONT LEFT CORNER)

Speed	Road Holding	Comfort	Power RMS
150km/h	+5.19%	+1.24%	291W
200km/h	+7.36%	+1.6%	384W
250km/h	+8.14%	+1.79%	629W

TABLE III

FULL CAR RESULTS: DIFFERENT ROUGHNESSES (FRONT LEFT CORNER)

IRI	Road Holding	Comfort	Power RMS
2	+9.37%	+2.13%	224W
3.5	+7.36%	+1.6%	384W
5	+5.64%	+1.22%	477W

TABLE IV

FULL CAR RESULTS: DIFFERENT AIRFOIL SURFACES (FRONT LEFT CORNER)

Surface	Road Holding	Comfort	Power RMS
0.05 m^2	+3.78%	+0.75%	377W
0.1 m^2	+7.36%	+1.6%	384W
0.15 m^2	+10.78%	+2.26%	398W

The quarter car has also been analyzed. The same experiments as the full car have been performed (vehicle speed, road roughness and airfoil surface variations), with the results listed in Table V, VI and VII. The results are unvarying with respect to the full car, thus showing the validity of the choice of the control-oriented model employed in Section II-A

V. CONCLUSIONS

An active aerodynamic surfaces control scheme to improve vehicle road holding capabilities has been presented. It has been shown that the vehicle road holding can be improved up to +10.78%, (+7.36% in nominal conditions) without negatively affecting comfort. In terms of requested power the analyzed system can be considered a middle ground between semi-active and active suspensions, as a semi-active suspension requires approximately 50W, while a full active suspension 1.5-7 kW. The presented application needs 200-600W (384W in the nominal case), and it has been demonstrated that it can improve road holding performance without affecting (indeed improving) the passengers' comfort, contrary to the semi-active and active suspensions. A

TABLE V

QUARTER CAR RESULTS: DIFFERENT VELOCITIES

Speed	Road Holding	Comfort	Power RMS
150km/h	+5.35%	+1.31%	280W
200km/h	+7.41%	+1.71%	375W
250km/h	+8.39%	+1.87%	596W

TABLE VI

QUARTER CAR RESULTS: DIFFERENT ROUGHNESSES

IRI	Road Holding	Comfort	Power RMS
2	+9.45%	+2.3%	210W
3.5	+7.41%	+1.71%	375W
5	+5.8%	+1.34%	467W

TABLE VII

QUARTER CAR RESULTS: DIFFERENT AIRFOIL SURFACES

Surface	Road Holding	Comfort	Power RMS
0.05 m^2	+3.82%	+0.81%	368W
0.1 m^2	+7.41%	+1.71%	375W
0.15 m^2	+10.85%	+2.4%	390W

second advantage is that the proposed architecture can be employed in coordination with other (semi-)active suspension strategies.

This study served as a analysis of the potentials of this strategy. Several issues still need to be addressed before being able to implement and test the strategy. The biggest hurdle is represented by technological aspects. Current work is focused on the mechanical implementation of the proposed active aerodynamic surfaces.

REFERENCES

[1] A. Savkoor and H. Happel, "Aerodynamic vehicle ride control with active spoilers," in *Proceedings of International Symposium on Advanced Vehicle Control*, 1996, pp. 647–682.

[2] A. Savkoor and C. Chou, "Application of aerodynamic actuators to improve vehicle handling," *Vehicle System Dynamics*, vol. 32, no. 4-5, pp. 345–374, 1999.

[3] C. Spelta, D. Delvecchio, R. Cantoni, R. Lazzari, and S. Savaresi, "Analysis and design of handling-oriented control strategies for semi-active suspensions," in *Decision and Control, 2009 held jointly with the 2009 28th Chinese Control Conference. CDC/CCC 2009. Proceedings of the 48th IEEE Conference on*. IEEE, 2009, pp. 7633–7638.

[4] S. Savaresi, C. Poussot-Vassal, C. Spelta, L. Dugard, and O. Sename, *Semi-active suspension control design for vehicles*. A Butterworth-Heinemann Title, 2010.

[5] I. Abbott, A. Von Doenhoff, and L. Stivers Jr, "Summary of airfoil data," Tech. Rep., 1945.

[6] J. Leishman, *Principles of helicopter aerodynamics*. Cambridge Univ Pr, 2006.

[7] R. Rotenberg, "Vehicle suspension," *Moskou: Mašinostrojenie (in Russian)*, 1972.

[8] W. Paterson, "International roughness index: Relationship to other measures of roughness and riding quality," *Transportation Research Record*, no. 1084, 1986.

[9] G. Koch, T. Kloiber, E. Pellegrini, and B. Lohmann, "A nonlinear estimator concept for active vehicle suspension control," in *American Control Conference (ACC), 2010*. IEEE, 2010, pp. 4576–4581.

[10] D. Delvecchio, C. Spelta, and S. Savaresi, "Estimation of the tire vertical deflection in a motorcycle suspension via kalman-filtering techniques," in *Control Applications (CCA), 2011 IEEE International Conference on*. IEEE, 2011, pp. 532–537.

[11] S. Skogestad and I. Postlethwaite, *Multivariable feedback control: analysis and design*. Wiley, 2007, vol. 2.